Available online at www.sciencedirect.com

ScienceDirect

journal homepage: http://www.elsevier.com/locate/acme

Original Research Article

Experimental and numerical investigation of the effect of the combined mechanism of circumferential expansion and folding on energy absorption parameters

Mostafa Abolfathi, Ali Alavi Nia *, *Ali Akhavan Attar, Mohammad Abbasi*

Department of Mechanical Engineering, Bu-Ali Sina University, Hamedan, Iran

ARTICLE INFO

Article history:
Received 15 January 2018
Accepted 20 May 2018
Available online 23 July 2018

Keywords:
Combined mechanism
Circumferential expansion
Folding
Simulation
Thin wall structure

ABSTRACT

In this research, in order to increase energy absorption of thin-walled tubes, a combined deformation mechanism is proposed which involves the simultaneous combination of circumferential expansion and folding. Such a combined mechanism was not concerned in the literature. The study is carried out both experimentally and numerically. A special device was designed and made to conduct experimental tests on tubes. The samples were made of aluminum, and quasi-static loading was applied at two different speeds of 10 and 200 mm/min. Energy absorption parameters including specific energy absorption (SEA), crushing mean force, initial peak force, the deformation mode and crush force efficiency (CFE) were studied. Experimental results showed that combined mechanism (without lubrication) could increase absorbed energy up to 123% compared to the folding mechanism. If the lubricant is used, the increase will be up to 97%. The combined deformation mechanism (without lubrication) increases absorbed energy up to 94% compared to the circumstantial expansion. This value will be 107% with lubrication. In addition, the initial peak force in the combined mechanism decreases between 8% and 36% relative to the folding mechanism. The circumstantial expansion in the proposed mechanism is complete and the expansion stroke length is 100%, while this stroke was less in the previous researches due to design restrictions. Numerical simulations were conducted using LS-Dyna software and there is good agreement between the numerical results and experimental data.

1. Introduction

Today, a variety of thin-walled structures are used as energy absorber in order to protect structures and withstand the destructive effects of impact under different conditions. Extensive research in this context has so far been carried out through analytical, numerical and experimental methods. These parts absorb the impact energy in different ways including lateral collapse [1–3], inversion [4,5], bending [6] and

* *Corresponding author.*
E-mail address: alavi495@basu.ac.ir (A. Alavi Nia).
https://doi.org/10.1016/j.acme.2018.05.004
1644-9665/

splitting [7]. Among the various types of collapse, two methods of axial collapse or folding and circumferential expansion are considered in this research.

In the study of energy absorption by circumferential expansion, an expansion mechanism with rigid die and ductile tube was suggested for the first time by Eddins [8] for the aircraft landing system.

Deformation in the form of circumferential expansion of cylindrical thin-walled tubes as an energy absorber was experimentally and numerically studied by Shakeri et al. [9]. In this work, a rigid tube is plunged into the thin-walled tube under axial pressure load. In this case, the impact energy is absorbed as expansion energy consumed by plastic work done on the ductile tube as well as frictional energy between the contact surfaces of two tubes. They showed that the mean crushing force can be affected by the thickness and tolerance between the rigid tube and the absorber tube, and the amount of friction coefficient. Due to the circumferential expansion, energy absorption of tubes was experimentally and numerically investigated by Yang et al. [10]. According to their results, the contribution of friction in the energy absorption of circumferential expansion was 22% of total absorbed energy. Also, for the tubes with smaller thickness, the expansion process occurs faster; moreover, in this case there is more contact between surfaces. In another work by Yan et al. [11], several mandrels were made with tip angles of 5–40 degrees and friction coefficients were considered from zero to 0.3 to acquire the appropriate angle of mandrel tip and friction coefficient. They proved that the relationship between the expansion angle and the loading force is nonlinear, while the coefficient of friction and the loading force have linear relation with each other. They reported the most appropriate angles for expansion between 10 and 20 degrees. As an energy dissipation mechanism, circumferential expansion of cylindrical tubes was experimentally and numerically investigated by Tavakoli [12].

Some theoretical works have been done in the field of energy absorption due to axial collapse [13–15]. Also, several studies have been conducted to study the effect of geometric parameters of energy absorber [16,17], quasi-static or dynamic loading as well as the effect of impact velocity [18–20] and the use of composites for the production of energy absorbers [21].

In addition, design and geometry of the energy absorber structure have been of interest to improve energy absorption in axial collapse deforestation. For example, changing the geometry of the tube section [22], making tubes with variable thickness [23,24], creating grooves and controlling buckling [25,26], adding internal and external stiffeners to the structure [27], use of glass-epoxy coating for the metal tube [28], the use of multi-cell absorbers [29,30], creation of circumferential and axial folding on the tube [31] and use of nested tubes as an energy absorber structure [32,33] are some of the changes that improve energy absorption in axial collapse.

Experimental investigations on the energy absorption in the process of shrinking–splitting of a cylindrical tube were carried out by Tanaskovic et al. [34]. In their study, energy absorption is performed by plastic deformation and the friction between the tube and the rod. After passing the cone section, the tube changes its way in the opposite direction of the splitter and more energy is lost during the process. The results showed that the combined absorber increases absorbed energy up to approximately 60% relative to shrinking absorber alone. Experimental and numerical study on energy absorption of cylindrical tubes in the expanding–splitting process was performed by Li et al. [35]. According to their research, the deformation involved two phases. The first phase of deformation included tube expansion by cylindrical mandrel and the second phase included the splitting of the expanded tube along with the initial scratches by the conical section of mandrel. Quasi-static compression test indicated that this kind of combined energy absorber increases the absorbed energy 95.34% relative to purely expansion deformation.

The main purpose of the present study is to provide a combined deformation mechanism that has larger energy absorption compared to two the previously introduced combined mechanisms. In previous studies, two mechanisms of shrinking–splitting and expansion–splitting have been discussed. In this research, combined mechanism energy absorption including circumferential expansion and folding was studied. Aluminum tubes with a suitable ductility were used as energy absorbers and axial quasi-static loading of structures was carried out. To do the loading, a special fixture was designed and built to do the two processes together. In addition to experimental tests, a numerical simulation was also done by finite element software LS-Dyna.

2. Experimental tests

2.1. *Specifications of samples*

Tests samples, in the form of a thin aluminum cylinder with an outer diameter of 70, thickness of 0.6, length of 107 mm, and mass of 102 g, were used. Chemical composition of the samples which has been determined by quantometery test based on ASTM E826 standard [36] is presented in Table 1. According to reference [37], the tube material is close to the aluminum alloy of the 1100 series.

To ensure the ductility of the tube, tensile test with a speed of 2 mm/min was performed. Fig. 1 shows tensile test samples according to ASTM E 8M standard [38] before and after the test. Engineering stress–strain curve obtained from the tensile test as well as the true stress–strain curve is indicated in Fig. 2.

2.2. *Design and manufacture of the fixture and the method of its usage*

One of the important parts of this research is designing a device that performs combined process of energy absorption in the desired form. Expected combined process is carried out by a mandrel with a rigid support attached to the end of it. Tubes with specified dimensions were expanded circumferentially at first, then, expanded tube was axially crushed.

The initial design of the fixture was prepared in Solidworks software (Fig. 3) and after ensuring its ability to work properly, designing components were made with proper tolerances. This apparatus has a mass of 24 kg and its overall dimensions are ($280 \times 280 \times 580$ mm). Components of the device are shown in Fig. 4.

Making mandrel both in terms of expansion diameter and cone angle requires high precision. Moreover, its material

Table 1 – Chemical composition of the tube material.

Si	Fe	Cu	Mn	Mg	Cr	Ni	Zn	Ti	Be	Ca	Li
0.38	0.86	0.1	0.06	0.12	Trace	Trace	0.11	0.02	Trace	0.002	Trace
Pb	Sn	Sr	V	Na	Bi	Co	Zr	B	Ga	Cd	Al
0.02	<0.005	Trace	0.01	Trace	0.01	0.005	Trace	0.01	Trace	0.003	Base

Fig. 1 – Tension test samples before (left) and after (right) test.

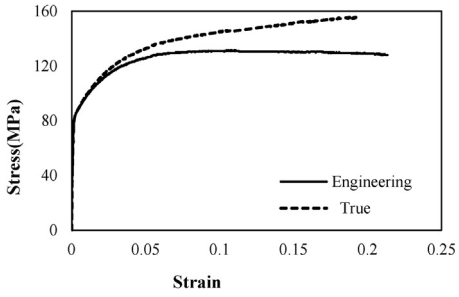

Fig. 2 – Stress–strain curves of the tube material.

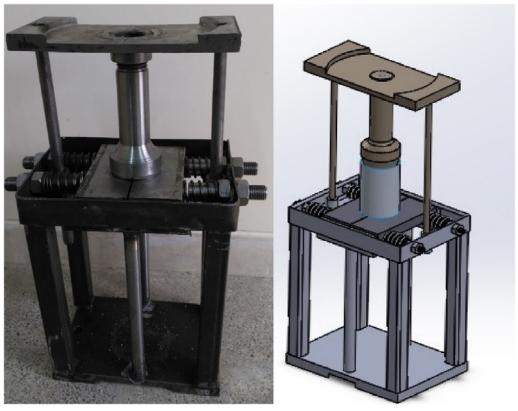

Fig. 3 – Designed (right) and built (left) fixture.

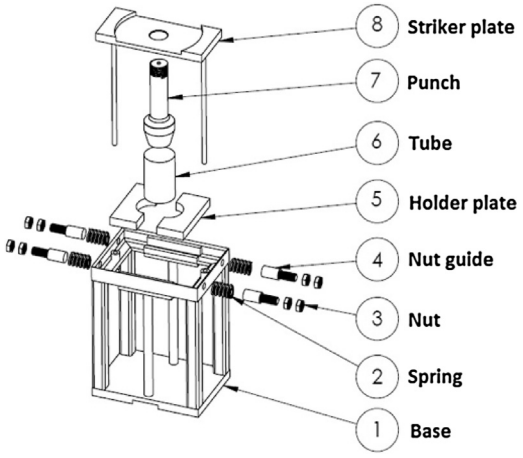

Fig. 4 – Exploded parts of the fixture.

must be hard enough to have the adequate resistance against corrosion. The mandrel was selected from the VCN steel, which is very hard. Cone angle was 15 degrees relative to the mandrel axis. Selection of this angle has been done according to the study by Reid and Harrigan [4] who reported the appropriate angle for an expansion between 10 and 20 degrees. The diameter of the expanding part was 70.8 mm and the small diameter of the mandrel was 40 mm. The smaller diameter of this section yields to easy exit of the crushed tube.

Performing a combined process is as follow:

Mandrel is firstly penetrated into the tube by the axial pressure and expands the tube, during the ending phase of expansion, the tip of the mandrel swerves the plates on which the tube is located and passes through it. These plates are controlled by springs to swerve up to the desired size. The length of the mandrel was adjusted in such a way that it would be a time interval for beginning of folding in case that mandrel passed between plates. At this time interval, the plates return to the first place and the bottom of the tube should hold the tube in the beginning of loading from the side of the pounding plates. Finally, the ultimate loading is done and the tube is crushed to the end.

To show the effect of friction in the process, the surfaces between the tube and the mandrel were lubricated in some cases by ordinary grease (Grease MP NLGI-3).

3. Tests and results

Axial loading tests on the tubes were performed by STM 150 kN (15 tons) apparatus at two loading speeds of 10 and 200 mm/

Fig. 5 – Santam apparatus with installed fixture.

min. Jaw displacement of machine for combined mode was 250 mm. Installed fixture on the Santam machine before loading is depicted in Fig. 5. To ensure the repeatability of the results, each test was performed on two similar samples. For combination mode, the effect of the lubricant was also studied. After taking the force–displacement diagram, the specific energy absorption (SEA) was calculated.

The SEA is calculated by dividing the absorbed energy by effective mass (the mass of the crushed part of the tube). Crushing steps for the process of the folding state are indicated in Fig. 6 while deformation stages for the combined deformation mode are shown in Fig. 7.

To clarify the effect of the combined deformation mechanism of circumferential expansion and folding, the results of this mechanism should be compared with the folding mechanism alone. Also, the effect of loading speed and lubrication on these processes should be checked out. Thus, the test plan was prepared as Table 2 which contained 6 absorber types. Meanwhile, two identical samples of any type were prepared and tested.

In samples' code in Table 2, the first letter specifies deformation mode (F for folding and C for combination) and the next number states the loading speed (mm/min); the letter "N" indicates a test without lubrication and the letter Y shows that the lubricant has been used in the test. Since two tests have been performed for each sample type, numbers 01 and 02 were dedicated to illustrate these two tests.

The results of the experiments represented that combined mechanism relative to folding mechanism increases absorbed energy from 1.43 to 3.19 that is about 123%. This amount is from 1.43 to 2.8 that is about 97% in lubrication mode; however, the lubricant's contribution is 26%. Also the combined mechanism leads to 81% increase in energy absorption (from 1.76 to 3.19) relative to the circumferential expansion. This amount is from 1.38 to 2.8 that is about 103% in lubrication mode.

4. Simulation

Simulations were performed using LS-Dyna explicit code and all experimental conditions were considered in simulation.

4.1. *Geometric model*

The model of the problem has three parts including mandrel, tube and retaining plate. The desired dimensions of these parts are shown in Fig. 8.

8515 shell elements were used in simulation of tube by the formulation of Belytschko-Tsay. Finite element models are

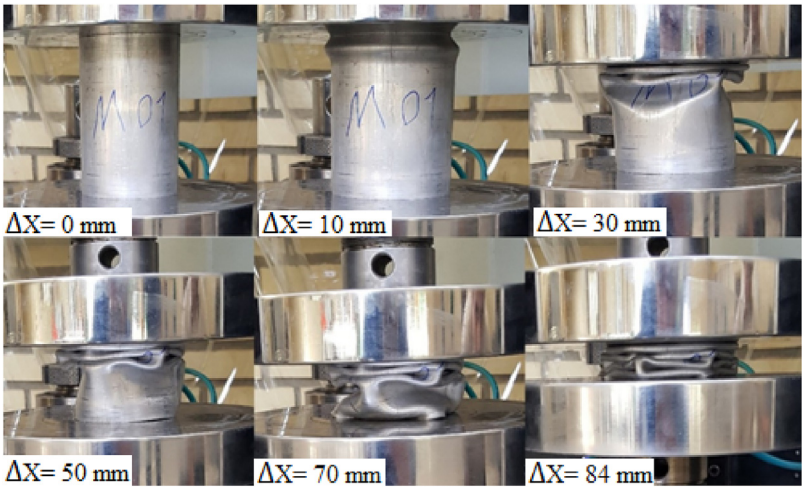

Fig. 6 – Consecutive steps of sample deformation in folding mode (F200N01).

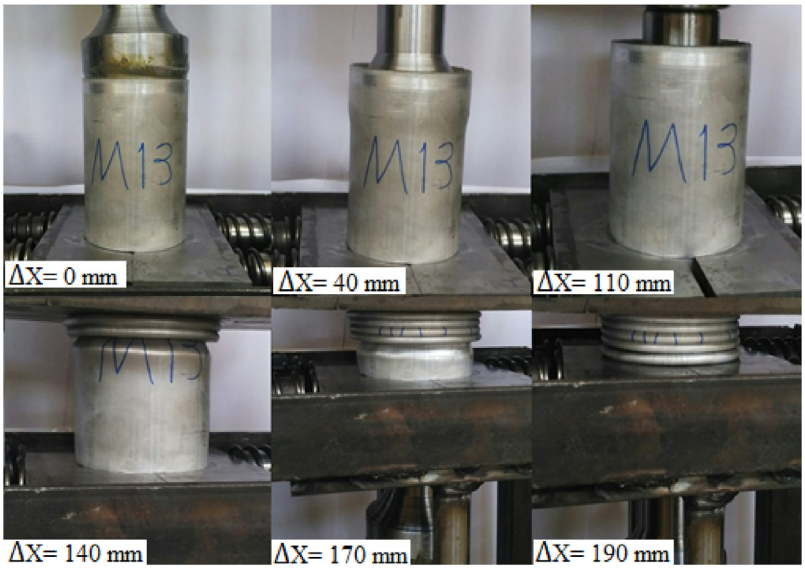

Fig. 7 – Consecutive steps of sample deformation in combined mode (C200Y01).

Table 2 – Various cases of tests and their codes.

Raw	Code	Loading rate (mm/min)	Lubrication	Deformation mode
1	F200N01	200	–	Folding
2	F10N01	10	–	Folding
3	C200N01	200	–	Combined
4	C200Y01	200	Done	Combined
5	C10N01	10	–	Combined
6	C10Y01	10	Done	Combined

shown in Fig. 9 for folding and combined deformations. To ensure the reliability of the response and sufficient number of elements, the problem was analyzed with a different number of tube elements and absorbed energy was selected as the sensitive parameter. Changes in absorbed energy due to the change in the number and size of the elements are presented in Table 3.

4.2. *Properties and boundary conditions*

Mandrel and retaining support were made of steel, and they have no deformation in this process. Therefore, the rigid material model with a density of 7800 kg/m^3, Young's modulus of 210 GPa and Poisson's ratio of 0.3 was attributed to these two parts. Material model of Piecewise-Liner-Plasticity was selected for aluminum tube with a density of 2700 kg/m^3, Young's modulus of 69 GPa, the Poisson ratio of 0.3 and the yield stress of 82.5 MPa. Also, the true stress–strain curve was considered for the tube in accordance with Fig. 2. The Automatic_Surface_To_Surface was considered for the contact between the mandrel and tube as well as between the bottom plate and the tube. Also, Automatic_Single_Surface was taken into account for the tube itself. The coefficient of friction was considered 0.45 in non-lubricating state and 0.25 for lubricating state [10]. In the definition of boundary conditions, the support was fully clamped and mandrel was also constrained in all directions except the vertical one. The tube was located between mandrel and the support. Loading is applied by the mandrel which moves down vertically. The retaining plate is fully constrained and is with contact with the tube. There is no any constraint for the tube and it can deform in any direction.

The upper mandrel moves with experimental loading speed, expands the tube at first and then crushes it. Progress of mandrel continues until formation of a state of rigidity for a crushed tube so that no further deformation of the tube is possible. This rigid state is specified with an instantaneous and intense increase in the slope of the ending part of the force–displacement diagram. Two types of samples collapse in combined mode are shown in Fig. 10. Loading rate is different for these samples, 200 mm/min and 10 mm/min for the cases "a" and "b", respectively. It should be noted that the symmetric and asymmetric deformation modes in thin-walled energy absorbers are a random process [39].

5. Results and discussion

5.1. *Investigation of folding deformation*

To illustrate the improvement rate of energy absorption for special combined process, it is required to compare the process with a separate deformation mode like folding. For this purpose, test for folding alone was also done. In the simulation section, deformation of folding was also reviewed and

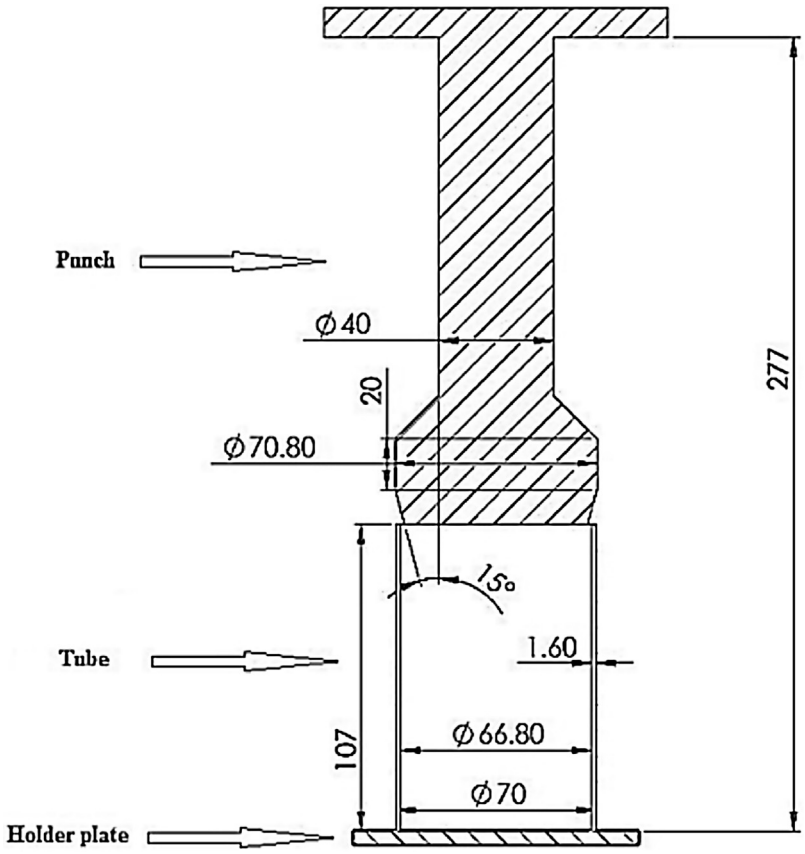

Fig. 8 – Geometric model of mandrel, tube and retaining plate (dimensions in mm).

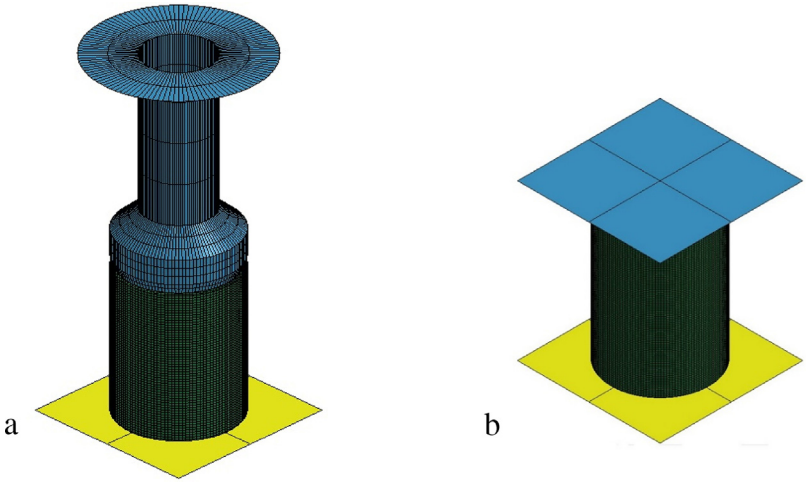

Fig. 9 – Finite element model for (a) combined mode and (b) folding mode.

compared with experimental results. In Fig. 11, force–displacement and energy–displacement diagrams related to collapse as folding were represented in both experimental and numerical modes. The main difference between the force–displacement diagrams is that the experimental state diagram is higher than the diagram of simulation mode. The reason can be error in measuring the tube thickness and possible anisotropy in the tube. Also, the slight change in thickness in various points of the tube, considering construction conditions, can be an error factor. As a result, in the case of being crushed, sample has a somewhat distance from regular conditions of folding which is imagined with formation of plastic hinges for it. This will further exacerbate this difference.

Table 3 – Energy absorption (EA) of the tube with different number of elements.

Case	Number of elements	Size of elements (mm)	EA (kJ)
1	312	8.8	3.32
2	465	7.0	2.95
3	820	5.4	3.14
4	1830	3.6	2.90
5	3240	2.7	2.70
6	5050	2.1	2.90
7	8515	1.6	2.90
8	12,480	1.3	2.90

Force–displacement diagrams in Fig. 11a were drawn for loading speed of 200 mm/min in which asymmetric collapse has occurred. Fig. 11b shows the corresponding energy graph. In addition, the graphs in Fig. 11c were depicted for loading speed of 10 mm/min in which collapse has occurred symmetrically and Fig. 11d indicates the corresponding energy diagram. It should be noted that the mandrel stroke in simulation mode is more than experimental state which is also due to the regularity of its collapse in simulation and the use of shell element in tube simulation. Energy–displacement diagrams were compared in Fig. 11. The difference seen in the ending section of the diagrams is due to the slight difference in how it collapses or the variance during the crushing or mandrel progress.

Numerical and experimental results were compared with more details in Table 4. In this table, energy absorption parameters such as mean force, peak force, absorbed energy, specific energy absorption, stroke, stroke efficiency (length of progress to tube length ratio) and crush force efficiency (mean force to maximum force ratio) were compared with each other

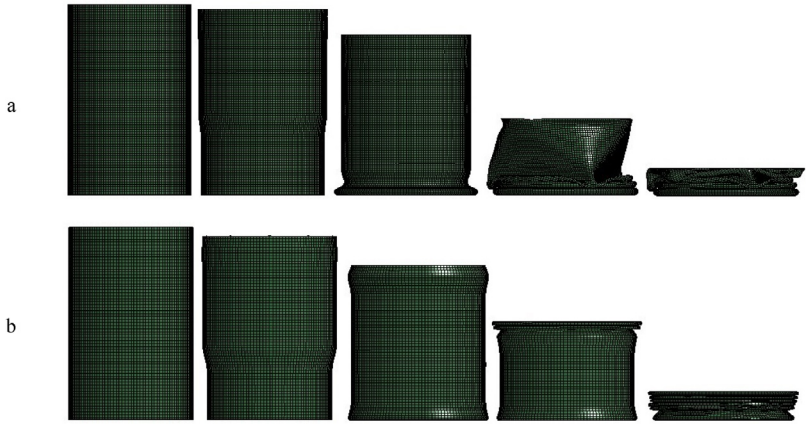

Fig. 10 – Consecutive steps of collapse of the tube in combined mode (simulation). (a) Asymmetric collapse from lower end (C200Y01). (b) Symmetric collapse from top end (C10Y01).

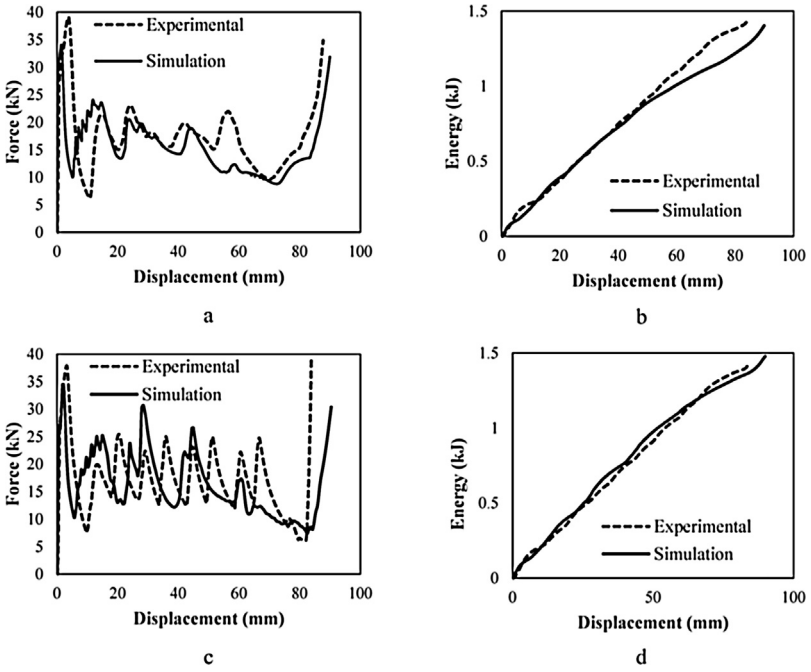

Fig. 11 – Experimental and numerical force–displacement and energy–displacement curves for folding deformation. (a and b) 200 mm/min loading rate. (c and d) 10 mm/min loading rate.

Table 4 – Energy absorption characteristics of tube in folding mode.

Specimen		Mf (kN)	Pf (kN)	EA (kJ)	SEA (J/g)	St (mm)	CFE %
F200N02	Experiment	17.0	36.8	1.43	14.0	84.0	46.0
	Simulation	16.4	34.4	1.48	14.5	89.4	47.5
	Difference %	3.5	6.5	3.50	3.5	6.4	3.2
F10N02	Experiment	16.9	37.6	1.45	14.2	85.8	44.8
	Simulation	15.6	34.1	1.40	13.7	89.0	45.7
	Difference %	7.4	9.3	3.40	3.4	3.6	2.0

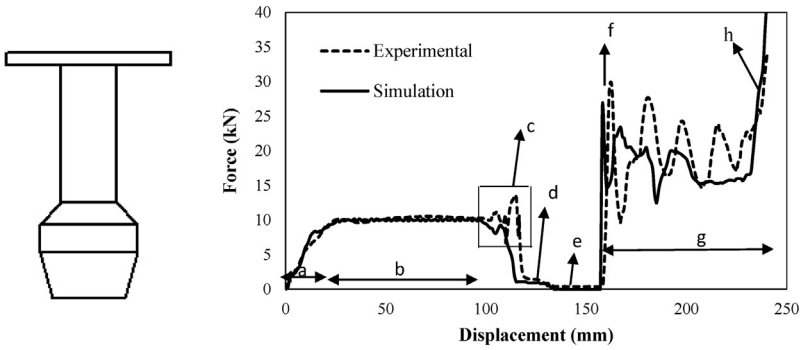

Fig. 12 – Different sections of load–displacement curves of C10Y02 sample in combined mode (experimental and numerical) (right), and the mandrel (left).

for numerical simulations and experimental tests. Generally, the force–displacement diagram is stopped where the gradient of the curve is very high. This point is known as the absorber crushing length. The length of crushing is affected by the collapse patterns. It can be seen that experimental and simulation results are well matched together.

5.2. *Examining combined deformation*

The main purpose of this research was to introduce a combined mechanism for circumferential expansion and simultaneous folding of the tube. The effect of this mechanism on improving energy absorption was examined at first by performing experimental tests. Then the obtained outcomes were used to validate simulation results. Then, the results of numerical simulation and experimental data were compared in a combined mode.

5.2.1. *Combined process analysis*

Force–displacement diagram in the combined process has different sections (Fig. 12). Expander mandrel is located in the left side of this figure and the force–displacement curve is placed on the right on which 8 major areas have been shown. The descriptions of these eight areas are as follows:

1. Section a: This section indicates the beginning of the expansion process by mandrel. The beginning of the section is the start of contact between the angled part with the tube while its ending point is where the inner diameter of the tube has reached to its final value i.e. the diameter of the mandrel. In this section only the upper part of the tube is expanded and then, becomes angled like the tip of the mandrel. Based on this section, it is observed that force must be exerted based on the end of the section (a) to change the diameter from an initial value to the diameter of the mandrel (for example, 10 kN for Fig. 12).
2. Section b: Since the initial diameter of the tube is constant at its length, the same force is required during the collapse for all parts of the tube to reach the diameter of the mandrel. Constant collapse force in various displacements of the mandrel leads to the creation of a horizontal part in the force–displacement curve. This force is referred to as a steady force (Sf) for expansion.
3. Section c: This area corresponds to a decrease and then a sudden increase but with a small amount in the force–displacement curve. In other words, after passing the uniform phase of b, the curve has slightly come down and then a jump occurs in the diagram. The cause of the lowering the force is the completion of the expansion stage of the tube. The reason for the jump in the curve is the surplus force that is consumed to overcome the friction caused by relative motion between tube and bottom surface. This relative movement is due to the matter that the end of the tube should slide on the lower rigid plate to reach the diameter of the mandrel which has not existed before.
4. Section d (interval between end of expansion and end of contact): After the removal of mandrel contact with the expanded parts, the material tends to compensate part of its deformation, that is, elastic deformation or spring back. Elastic deformation recovery in the expanded sections, which has no constraint at present, affects bounded parts. In this way, at the contact surface of the mandrel with the

tube, a force is exerted into the mandrel. This force always exists in expansion (area b) between the mandrel and the tube but since the amount of this force is low, it is specified when the expansion of the tube is finished and mandrel and tube are still in contact with each other. It is important to know that the angle of mandrel tip affects this issue so that whatever the angles of the tip of the mandrel are higher, the area d is placed at a lower level.

5. Section e: In this area, expansion of tube as well as the contact between the mandrel and the tube has ended; therefore, as long as the top plate of the mandrel does not reach the tube, the amount of force in the force–displacement curve is zero.
6. Section f: This area represents the beginning of the folding in expanded tube and corresponds to a force jump in the curve because of the initial elastic deformation. During folding process in a tube, institution of the first plastic hinge requires the most force.
7. Section g: This area indicates the collapse of the tube in the form of folding. Number of peaks in this area corresponds to the number of folds created in the tube.
8. Section h: Ending part of diagram is accompanied with a steep and sudden increase. That is, the tube is completely crushed at this time.

5.2.2. *The results of the combined deformation*

An important point in combined mode results is ascending rate of expansion zone of the force–displacement diagrams (area b in Fig. 12) in experimental tests without lubricant. Because of the tube's ductility and the presence of friction, the inner surface of the tube is scratched with the mandrel development and sticks to its surface. This phenomenon causes gradually rise of friction in this area. Moreover, accumulated burrs on the surface of the mandrel raise surfaces interference. These two factors lead to an increase in the diagram in area b.

Force and energy graphs are in fact complementary. Placing these two graphs near each other makes the comparison clearer. Force–displacement diagrams as well as the energy–displacement of the four tested samples along with numerical simulation results are shown in Fig. 13. Figures a (without lubricant) and c (lubricated) are related to the loading speed of 200 mm/min and Figures e (without lubricant) and g (lubricated) are associated with the speed of 10 mm/min. Figures b, d, f and h are corresponding energy–displacement diagrams of a, c, e, and g cases, respectively. The beginning portion of energy–displacement diagrams, is related to the circumferential expansion of the tube, horizontal section (section b) is associated to the time interval, while the latter part is related to the folding process. Parameters extracted from force–displacement curves of the four mentioned samples in both simulation and experimental modes are compared in Table 5. It is seen that there is a good agreement between experimental and numerical results. Numerical simulation are carried out to insure the changes in force–displacement curves, various collapse modes and to clear the contribution of each portion of deformation on energy dissipation. Besides, the results explained in Section 5.2.2 for the combined deformation, will be more reliable.

Stroke efficiency is equal to the ratio of the deformed length of the tube to the tube length before deformation. The more the stroke efficiency, the more capability of the tube has used to absorb energy. In this work, the deformed length of the tube is considered for calculation of stroke efficiency. Since the tube length is deformed twice, therefore, efficiency is more than when the tube is only once deformed.

5.3. *Comparison of deformed samples*

In this section, four cases of crushed samples in experimental tests were compared with simulation results. As shown in Figs. 14 and 15, symmetric and asymmetric collapses have occurred for folding and combined deformation in tested tubes. Also, asymmetric, symmetric, and mixed collapse occurred in the simulation results.

5.4. *Effect of combined mechanism on improvement of absorbed energy*

Energy absorption in combined mode is compared with absorbed energy of individual circumferential mode or folding mode in this section. It should be noted that lubrication is not effective in the folding mode. Given the data in Fig. 16, it is specified that the energy absorption is approximately doubled by the combined mechanism. In this figure, absorbed energy of test samples at loading rates of 10 and 200 mm/min were compared in two cases including with and without lubricants. It is seen that when lubrication has not been done for loading at a speed of 200 mm/min, combined mechanism compared with normal folding increases energy absorption by 123% in which this amount will be 97% with lubrication, that is, the lubricant's share is 26%. Without lubrication at loading speed of 10 mm/min, combined mechanism compared to conventional folding increases energy absorption by 107%. This amount is 93% in lubrication mode and therefore, the lubrication share for this case becomes 14% in reduction of energy absorption. It is observed that the effect of lubrication is more at higher loading rate. Also, the combined mechanism results in 81% increase in energy absorption for speed of 200 mm/min in the lubrication mode compared to the circumferential expansion. This amount is 103% in lubrication mode and the lubrication share is 22%. Combined mechanism has 94% of increase in energy absorption relative to circumferential expansion for speed of 200 mm/min in which this value is 107% in lubrication mode and the lubrication share is 13%. From the above statements, several results are obtained as the following:

1. In the case of lubrication, folding mechanism absorbs more energy relative to circumferential expansion which is contrary in a non-lubricant state.
2. Combined process includes two parts: The expansion section is affected by friction and lubrication causes reduction in absorbed energy, and the folding section is independent from lubrication. Therefore, in case of comparing, lubrication in expansion has a greater impact than a combined mode.
3. The purpose of lubrication in the mechanism of circumferential expansion is the prevention of rupture and possible

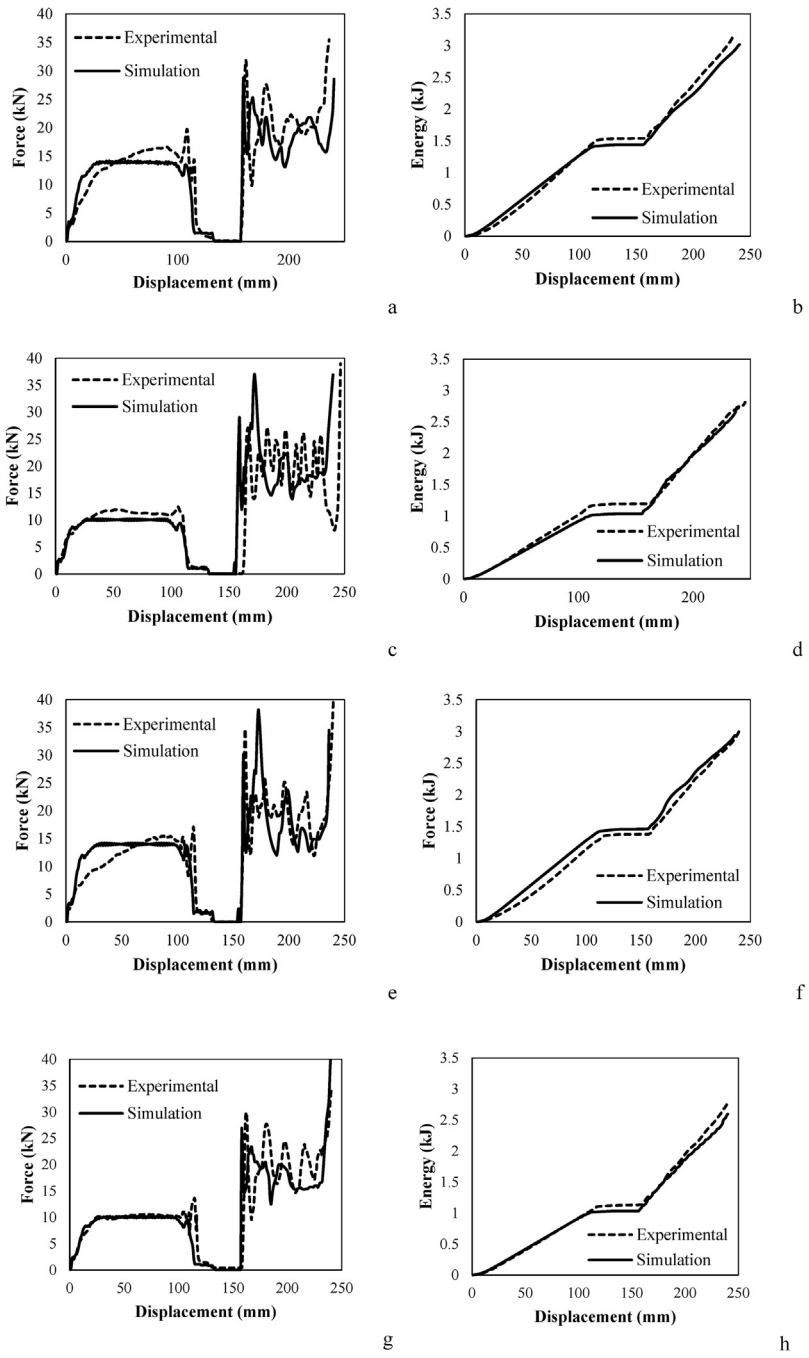

Fig. 13 – Experimental and numerical load–displacement and energy–displacement curves for combined mode of deformation. (a and b) 200 mm/min loading rate without lubrication. (c and d) 200 mm/min loading rate with lubrication. (e and f) 10 mm/min loading rate without lubrication. (g and h) 10 mm/min loading rate with lubrication.

damages of the tube during loading. Both loading rates in this research are in the quasi-static range. As it is clear from the results, energy absorption at these two speeds has little difference and that the general trend of results is the same at both speeds.

The peak force of samples in different experimental conditions has been investigated in Fig. 17. This force is an important parameter in energy absorbers and the less the force, the less the severity of the impact is felt in accidents. So far, different ways have been proposed to reduce the force.

In the combined mechanism, tube is converted to a barrel-shape form after expansion. This causes that maximum appeared force in this diagram is less than the initial tube's peak force which is only subjected to folding. Maximum force of combined mechanism, in the case where no lubricant is

Table 5 – Energy absorption characteristics of the samples in combined mode.

Specimen		Mf (kN)	Sf (kN)	Pf (kN)	EA (kJ)	SEA (J/g)	St (mm)	CFE %
C200N02	Experimental	13.9	14.4	31.9	3.19	31.3	81.0	43
	Simulation	15.2	14.0	29.6	3.02	29.6	87.0	48
	Difference %	9.3	3.0	7.2	5.30	5.3	7.4	11
C200Y01	Experimental	14.2	10.9	27.1	2.80	27.6	84.5	52
	Simulation	14.0	10.0	29.0	2.74	26.9	86.0	48
	Difference %	1.4	8.2	7.0	2.10	2.1	1.8	8
C10N01	Experimental	15.6	12.8	34.8	3.00	29.4	86.0	45
	Simulation	15.5	14.0	38.1	2.94	28.8	82.0	41
	Difference %	0.6	9.3	9.5	2.00	2.0	4.6	9
C10Y02	Experimental	13.1	10.2	29.0	2.80	27.5	83.5	43
	Simulation	13.5	10.0	26.4	2.59	25.4	86.0	51
	Difference %	3.0	2.0	8.8	7.50	7.5	3.0	18

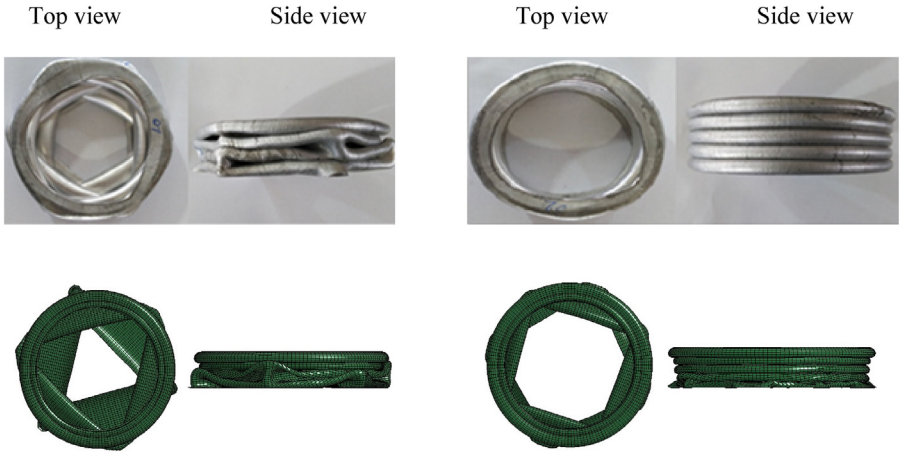

Fig. 14 – Deformed shape of two samples in folding mode (up experimental and down simulation).

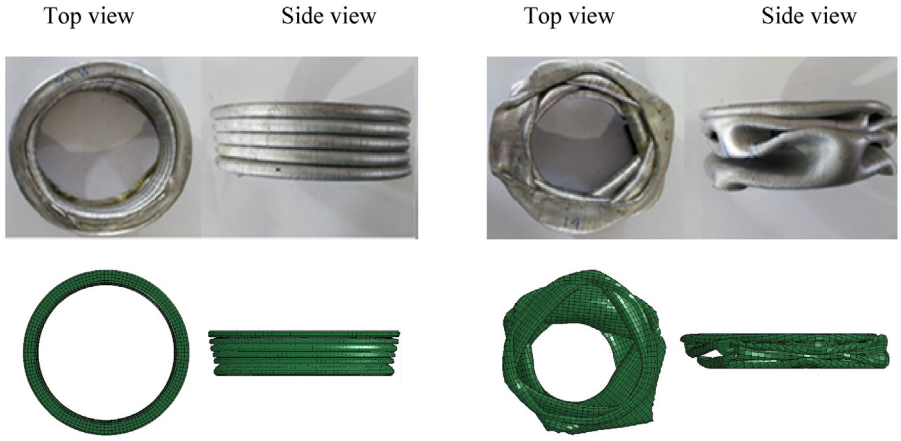

Fig. 15 – Deformed shape of two samples in combined mode (up experimental and down simulation).

used, has become more than the case where lubricant is applied. Also, quasi-static loading at high speeds has greater maximum force relative to low speeds.

In comparison of crush force efficiency (CFE), no particular change is observed between combined deformation and folding. Since part of energy absorption in combined mode is related to the circumferential expansion which has a lower mean force compared to folding, the mean force for folding is in general greater than the combined deformation. On the other hand, the maximum force is less in combination mode.

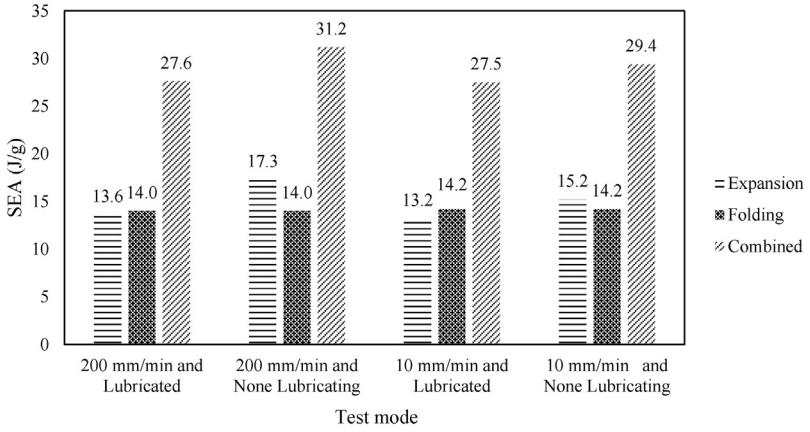

Fig. 16 – Comparison of SEA for three different modes of deformation.

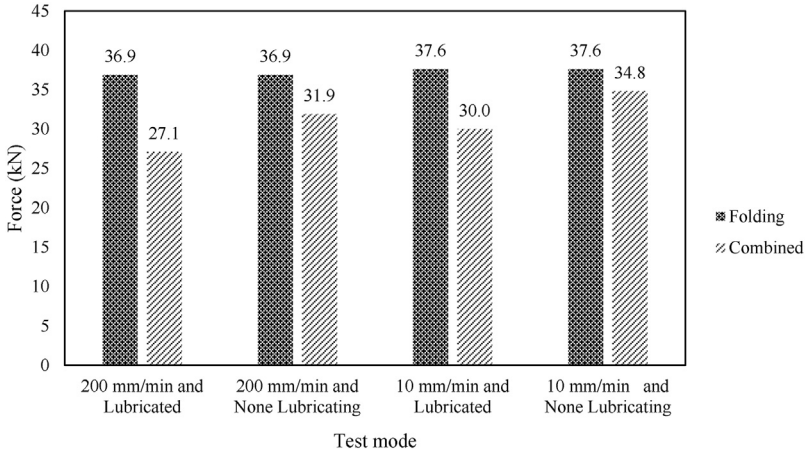

Fig. 17 – Comparison of peak force for combined mode and folding mode of deformation.

With the mentioned interpretations, the crush force efficiency is ultimately equal for two modes.

6. Conclusion

The purpose of the present study was to investigate the energy absorption characteristics and mechanical behavior of thin-walled aluminum cylindrical tubes under axial loading in a way that structure deformation is a combination of circumferential expansion and folding. Applying this type of collapse requires that a mechanism be designed which has the capability of doing so. Therefore, the desired fixture was designed and built. Thin-walled aluminum tubes were prepared and their mechanical properties were determined by standard tests. Then, given the effective parameters, the test plan was arranged and experimental samples were then tested. Numerical simulation was conducted using LS-Dyna software and the results were compared with experimental data. Reviews revealed that simulation and experimental results are well matched with each other and the above-mentioned combined mechanism has an effective role in increasing energy absorption. The most important results of this research are as follows:

1. Combined deformation mechanism (without lubrication) increases the absorption of energy between 107% and 123% relative to folding alone. If the lubricant is used, this ratio will be 93–97%; as a result, the friction share in this comparison is 14–26%.
2. Combined deformation mechanism (without lubrication) causes rise in the rate of energy absorption between 81% and 94%, relative to the circumferential expansion. If the lubricant is used, this ratio will be between 103% and 107%; as a result, the friction contribution in this comparison is 13–22%.
3. Relative to folding, peak force in the combined mechanism is reduced about 8–36%.
4. Since the tube length is deformed twice in combined mechanism, therefore, efficiency is more than when the tube is only once deformed in folding or expansion deformation.
5. By applying the proposed process of this study, expansion deformation is completely done and stroke length of

expansion is 100%, while the mentioned length was less than 100% in previous research due to design constraints.
6. Crush force efficiency for combined deformation and folding is almost the same.

Ethical statement

Authors state that the research was conducted according to ethical standards.

REFERENCES

[1] A. Niknejad, S.A. Elahi, G.H. Liaghat, Experimental investigation on the lateral compression in the foam-filled circular tubes, Mater. Des. 36 (2012) 24–34.
[2] A. Niknejad, D.M. Rahmani, Experimental and theoretical study of the lateral compression process on the empty and foam-filled hexagonal columns, Mater. Des. 53 (2014) 250–261.
[3] A. Baroutaji, M.D. Gilchrist, D. Smyth, A.G. Olabi, Analysis and optimization of sandwich tubes energy absorbers under lateral loading, Int. J. Impact Eng. 82 (2015) 74–88.
[4] S.R. Reid, J.J. Harrigan, Transient effects in the quasi-static and dynamic internal inversion and nosing of metal tubes, Int. J. Mech. Sci. 40 (1998) 263–280.
[5] A. Niknejad, M. Moeinifard, Theoretical and experimental studies of the external inversion process in the circular metal tubes, Mater. Des. 40 (2012) 324–330.
[6] T.H. Kim, S.R. Reid, Bending collapse of thin-walled rectangular section columns, Comput. Struct. 79 (2001) 1897–1911.
[7] G. Lu, L.S. Ong, B. Wang, H.W. Ng, An experimental study on tearing energy in splitting square metal tubes, Int. J. Mech. Sci. 36 (1994) 1087–1097.
[8] T.O. Eddins, Space craft soft landing system, U.S. Patent 3181821 (1965).
[9] M. Shakeri, S. Salehghaffari, R. Mirzaeifar, Expansion of circular tubes by rigid tubes as impact energy absorbers: experimental and theoretical investigation, Int. J. Crashworthiness 12 (2007) 493–501.
[10] J. Yang, M. Luo, Y. Hua, G. Lu, Energy absorption of expansion tubes using a conical–cylindrical die: experiments and numerical simulation, Int. J. Mech. Sci. 52 (2010) 716–725.
[11] J. Yan, Sh. Yao, P. Xu, Y. Peng, H. Shao, Sh. Zhao, Theoretical prediction and numerical studies of expanding circular tubes as energy absorbers, Int. J. Mech. Sci. 21 (2015) 213–243.
[12] M.J. Tavakoli, Experimental and numerical investigation of energy absorption parameter of cylindrical tubes, (M.Sc. thesis), Bu Ali Sina University, 2014.
[13] J.M. Alexander, An approximate analysis of the collapse of the thin cylindrical shells under axial loading, J. Appl. Math. Mech. 13 (1960) 10–15.
[14] W. Abramowicz, N. Jones, Dynamic axial crushing of circular tubes, Int. J. Impact Eng. 2 (1984) 263–281.
[15] T. Wierzbicki, S.U. Bhat, W. Abramowicz, D. Brodkin, A two folding elements model of progressive crushing of tubes, Int. J. Solids Struct. 29 (1992) 3269–3288.
[16] J. Maa, D. Hou, Y. Chen, Zh. You, Quasi-static axial crushing of thin-walled tubes with a kite-shape rigid origami pattern: numerical simulation, Thin-Walled Struct. 100 (2016) 38–47.
[17] X. Zhang, H. Zhang, Crush resistance of square tubes with various thickness configurations, Thin-Walled Struct. 107 (2016) 58–68.
[18] Zh. Yang, H. Yan, C.H. Huang, X. Diao, X. Wu, S.H. Wang, L. Lu, L. Liao, Experimental and numerical study of circular stainless thin tube energy absorber under axial impact by a control rod, Thin-Walled Struct. 82 (2014) 24–32.
[19] C. Zhou, B. Wang, J. Ma, Zh. You, Dynamic axial crushing of origami crash boxes, Int. J. Mech. Sci. 118 (2016) 1–12.
[20] A. Alavi Nia, H. Khodabakhsh, The effect of radial distance of concentric thin-walled tubes on their energy absorption capability under axial dynamic and quasi-static loading, Thin-Walled Struct. 93 (2015) 188–197.
[21] H. Jiang, Y. Ren, B. Gao, J. Xiang, Numerical investigation on links between the stacking sequence and energy absorption characteristics of fabric and unidirectional composite sinusoidal plate, Compos. Struct. 171 (2017) 328–402.
[22] A. Alavi Nia, J. Haddad Hamedani, Comparative analysis of energy absorption and deformations of thin walled tubes with various section geometries, Thin-Walled Struct. 48 (2010) 946–954.
[23] M.E. Erdina, C. Baykasoglu, M.T. Cetina, Quasi-static axial crushing behavior of thin-walled circular aluminum tubes with functionally graded thickness, Procedia Eng. 149 (2016) 559–565.
[24] G. Sun, T. Pang, Ch. Xu, G. Zheng, J. Song, Energy absorption mechanics for variable thickness thin-walled structures, Thin-Walled Struct. 118 (2017) 214–228.
[25] S. Salehghaffari, M. Tajdari, M. Panahi, F. Mokhtarnezhad, Attempts to improve energy absorption characteristics of circular metal tubes subjected to axial loading, Thin-Walled Struct. 48 (2010) 379–390.
[26] Zh. Yang, Y. Yu, Y. Wei, Ch. Huang, Crushing behavior of a thin-walled circular tube with internal gradient grooves fabricated by SLM 3D printing, Thin-Walled Struct. 111 (2017) 1–8.
[27] A. Alavi Nia, A. Akhavan Attar, The effect of different layouts in internal and external stiffeners on the energy absorption of thin-walled structures with square sections, Arch. Civil Mech. Eng. 17 (2017) 997–1010.
[28] M. Mirzaei, M. Shakeri, M. Sadighi, H. Akbarshahi, Experimental and analytical assessment of axial crushing of circular hybrid tubes under quasi-static load, Compos. Struct. 94 (2012) 1959–1966.
[29] A. Alavi Nia, M. Parsapour, An investigation on the energy absorption characteristics of multi-cell square tubes, Thin-Walled Struct. 68 (2013) 26–34.
[30] A. Alavi Nia, M. Parsapour, Comparative analysis of energy absorption capacity of simple and multi-cell thin-walled tubes with triangular, square, hexagonal and octagonal sections, Thin-Walled Struct. 74 (2014) 155–165.
[31] M. Eyvazian, M. Habibi, A.M. Hamouda, R. Hedayati, Axial crushing behavior and energy absorption efficiency of corrugated tubes, Mater. Des. 54 (2014) 1028–1038.
[32] A. Alavi Nia, S. Chahardoli, Mechanical behavior of nested multi-tubular structures under quasi-static axial load, Thin-Walled Struct. 106 (2016) 376–389.
[33] M.J. Rezvani, B. Jafarian, An experimental investigation on energy absorption of thin-walled bitubal structures by inversion and axial collapse, Int. J. Mech. Sci. 126 (2017) 270–280.
[34] J. Tanaskovic, D. Milkovic, V. Lucanin, G. Vasic Franklin, Experimental investigations of the shrinking–splitting tube collision energy absorber, Thin-Walled Struct. 86 (2015) 142–147.
[35] J. Li, G. Gao, H. Dong, S. Xie, W. Guan, Study on the energy absorption of the expanding–splitting circular tube by

experimental investigations and numerical simulations, Thin-Walled Struct. 103 (2016) 105–114.
[36] A. International, ASTM E 826 Standard Practice for Testing Homogeneity of a Metal Lot or Batch in Solid Form by Spark Atomic Emission Spectrometry, ASTM, USA, 2009.
[37] A.S.M.I.H. Committee, Properties and Selection: Nonferrous Alloys and Special-Purpose Materials, ASM International, USA, 1990.
[38] A. International, ASTM E8/E8M – 09 Standard Test Methods for Tension Testing of Metallic Materials, ASTM, USA, 2009.
[39] D. Al Galib, A. Limam, Experimental and numerical investigation of static and dynamic axial crushing of circular aluminum tubes, Thin-Walled Struct. 42 (2004) 1103–1137.